

# Phonons in Epitaxial DySi<sub>2</sub>: From the Bulk to Self-Organized Nanoislands and Nanowires

Svetoslav Stankov<sup>1,2,\*</sup>, Przemysław Piekarczyk<sup>3,†</sup>, Anja Seiler<sup>2</sup>, Daniel G. Merkel<sup>4</sup>, Olga Bauder<sup>2</sup>,  
Ramu Pradip<sup>2</sup>, Tilo G. Baumbach<sup>1,2</sup>, Aleksandr I. Chumakov<sup>5</sup>, and Rudolf Ruffer<sup>5</sup>


<sup>1</sup>*Institute for Photon Science and Synchrotron Radiation, Karlsruhe Institute of Technology, Karlsruhe, Germany*

<sup>2</sup>*Laboratory for Applications of Synchrotron Radiation, Karlsruhe Institute of Technology, Karlsruhe, Germany*

<sup>3</sup>*Institute of Nuclear Physics, Polish Academy of Sciences, Kraków, Poland*

<sup>4</sup>*HUN-REN Wigner Research Centre for Physics, Budapest, Hungary*

<sup>5</sup>*ESRF-The European Synchrotron, Grenoble, France*

 (Received 7 September 2024; revised 31 October 2025; accepted 20 November 2025; published 17 December 2025)

Using nuclear inelastic scattering on <sup>161</sup>Dy, we determined the Dy-partial phonon density of states of epitaxial DySi<sub>2</sub> in bulk and self-organized nanoislands and nanowires (NWs) on vicinal Si(001) surface. Compared to the bulk, the nanoislands exhibit softening of the crystal lattice, which is further enhanced in the NWs and significantly affects their thermodynamic and elastic properties. Our *ab initio* calculations reveal that the origin of this effect is the vibrations of Dy atoms located at the surfaces of the nanoislands and the NWs as well as forming a (2 × 4) reconstruction on the Si(001) surface between the NWs. The results demonstrate that, opposite to the widely accepted anisotropic lattice mismatch model, the NWs form with their length along the [0001] direction of the strained hexagonal unit cell with lattice parameters close to the Si(001) surface.

DOI: 10.1103/4r3t-tr77

Being a fundamental characteristic of materials, lattice dynamics plays a decisive role for important properties like thermal and electrical conductivity, vibrational entropy, specific heat capacity, and phenomena such as superconductivity, thermoelectricity, and phase transitions, among others [1,2]. Owing to the broken translational symmetry at surfaces and interfaces, the enhanced surface- and interface-to-volume ratio, and the elastic strain, inherently present in thin films and nanostructures, their phonon dispersions and phonon density of states (PDOS), which characterize the lattice dynamics of a solid, undergo dramatic modifications [3]. These comprise shift, broadening, and suppression of the bulk-specific phonon states and emergence of surface- and interface-specific states [4–10]. Consequently, the interactions of phonons with electrons, magnons, and other phonons are significantly enhanced compared to the bulk counterparts [11,12]. Gaining full control over the phonons and their interactions has the potential to revolutionize important fields spanning thermoelectrics, thermal management of nanoelectronics, spintronics, and quantum computing and to enable efficient devices operating at terahertz

frequencies [13–16]. Tailoring vibrational properties by nanoscaling, which is the main objective of the phononics [19–17]], requires a fundamental understanding of the lattice dynamics at the nanolength scale that is an experimental challenge.

Self-organized metallic nano-objects such as nanoislands, nanoclusters, and high aspect ratio nanowires (NWs) have been at the center of extensive research driven by the continuous downscaling of the CMOS electronics that requires new approaches in the device architecture and circuits interconnects [20–22]. Since the first report by Preinesberger *et al.* [23], rare earth disilicide (RESi<sub>2</sub>) nanoislands and NWs have attracted considerable interest due to their high electric conductivity, low Schottky barrier height, remarkable chemical stability, self-organization in high-density nano-objects with tunable size and shape, and direct integration with Si technology [24–27]. In addition to their potential for applications in optoelectronics, light-emitting technology and nanoelectronics as waveguides [28], Ohmic contacts, and interconnects [29,30], the RESi<sub>2</sub> NWs have been a fruitful playground [31] for the investigation of quasi-one-dimensional electronic band structures [32–34], one-dimensional metallicity [35], and charge-order fluctuations [36]. Despite the thorough investigation of the RESi<sub>2</sub> nanostructures, reports about their lattice dynamics remain scarce [7,37].

The archetypal DySi<sub>2</sub> is among the most studied RESi<sub>2</sub> systems [23,25–27,33,38–44]. In the bulk, it adopts the slightly distorted orthorhombic GdSi<sub>2</sub>-type structure, which transforms at 540 °C to the tetragonal ThSi<sub>2</sub>-type structure,

\*Contact author: Svetoslav.Stankov@kit.edu

†Contact author: Przemyslaw.Piekarczyk@ifj.edu.pl

Published by the American Physical Society under the terms of the [Creative Commons Attribution 4.0 International license](#). Further distribution of this work must maintain attribution to the author(s) and the published article's title, journal citation, and DOI.

or the hexagonal  $\text{AlB}_2$ -type lattice [45–47]. These structures were also reported in thin films and nanoislands [39,48–51]. The NWs exhibit the hexagonal lattice and coexist with a Dy-induced  $(2 \times 4)$  and/or  $(2 \times 7)$  reconstructed  $\text{Si}(001)$  surface [52–54]. It has generally been accepted that the NWs form along the  $[11\bar{2}0]$  direction, due to the almost perfect lattice match with the  $\text{Si}(001)$  surface, whereas the large mismatch along the  $[0001]$  direction limits their width [24,25,38,40,55]. However, recent microscopic investigations of  $\text{TbSi}_2$  NWs indicate that they are formed along  $[0001]$ , which is likely to apply to the NWs based on the trivalent rare earth metals [56,57]. The elucidation of the crystallographic orientation is of primary importance for achieving a comprehensive understanding of the properties of the NWs and their tailoring for specific applications.

Here, we report a systematic lattice dynamics study of epitaxial  $\text{DySi}_2$  upon the transition from a bulklike crystal to self-organized nanoislands and NWs on the vicinal  $\text{Si}(001)$  surface. The Dy-PDOS of the nanoislands reveals softening of the crystal lattice, which is further enhanced in the NWs. Our *ab initio* calculations unveil the origin of this effect and demonstrate that the NWs grow along the  $[0001]$  direction of the strained hexagonal crystal lattice.

Epitaxial  $\text{DySi}_2$  samples with nominal Dy coverages of 71.4 ML [bulklike sample; one monolayer (ML) equals  $6.78 \times 10^{14}$  atoms per  $\text{cm}^2$ —the surface atomic density of the  $\text{Si}(001)$ ], 0.93 ML (nanoislands), and 0.35 ML (NWs), hereinafter referred to as A, B, and C, respectively, were prepared by deposition of metallic Dy, enriched to 96% in the Mössbauer isotope  $^{161}\text{Dy}$ , on the vicinal  $\text{Si}(001)$  surface with a miscut of  $4^\circ$  toward  $[110]$ . This substrate ensures the formation of uniaxially aligned NWs, as evidenced by atomic force microscopy (AFM) study [40,58]. The *in situ* nuclear inelastic scattering [60,61] experiment was performed in the ultrahigh vacuum system [62] at the Nuclear Resonance beamline ID18 [63] of the ESRF-The European Synchrotron using x-rays with an energy of 25.651 keV and an energy resolution of 1.0(1) meV [64]. The horizontal beam size was 1.4 mm, and the vertical beam size was reduced to 8  $\mu\text{m}$ . Samples A and C were investigated with the wave vector of the incident photons being parallel to  $\text{Si}[110]$  and  $\text{Si}[\bar{1}\bar{1}0]$ , whereas sample B was measured only along  $\text{Si}[110]$ . All samples were kept at 115 K during the measurements to reduce the multiphonon excitation and were illuminated with the x-ray beam at a glancing angle of ca.  $0.1^\circ$  ensuring that the in-plane-projected Dy-PDOS was determined [65,66].

Figure 1(a) shows the Dy-PDOS of the bulklike sample (A), nanoislands (B), and NWs (C) and the corresponding AFM images of identical samples obtained in the home lab [58]. Analysis of the surface morphology and crystal structure of sample A confirms the formation of an epitaxial bulklike crystal with tetragonal structure [58]. The AFM image [Fig. 1(b)] reveals that this sample consists of rectangular crystals with sizes of several tens to several

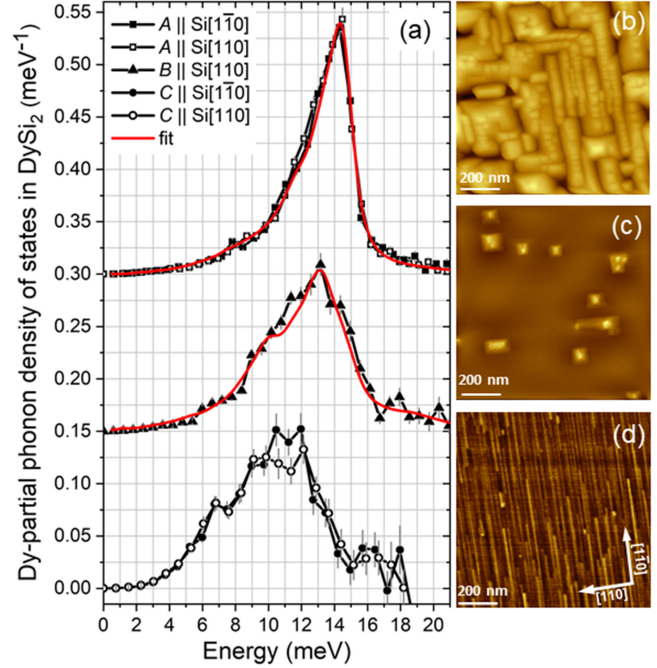


FIG. 1. (a) Dy-PDOS of the  $\text{DySi}_2$  bulklike sample (A), nanoislands (B), and NWs (C) obtained at 115 K with the wave vector of the x-rays being parallel to the indicated directions of the  $\text{Si}(001)$  surface (for clarity, the spectra are shifted by  $0.15 \text{ meV}^{-1}$ ). The solid red lines represent the fit (see the text for details). AFM images of identical bulklike (b), nanoislands (c), and NWs (d) samples obtained in the home lab.

hundreds of nanometers which coalesce together, forming a bulklike film with an average thickness of 45(5) nm and a high density of grain boundaries. The Dy-PDOS of sample A is characterized by a localized peak at 14.5 meV, low- and high-energy tails, and a cutoff at 19 meV. Similarly to the Eu-PDOS of tetragonal  $\text{EuSi}_2$  [7], this vibrational behavior corresponds to a rattling mode of the Dy atoms locked in a cage formed by the surrounding 12 Si atoms [45]. Compared to the Eu-PDOS, however, the peak is shifted by 2 meV to higher energy despite the fact that  $^{161}\text{Dy}$  is by 10 amu heavier from  $^{151}\text{Eu}$ . This shift is a consequence from the smaller atomic radius of Dy compared to Eu (lanthanide contraction [67,68]), which leads to reduced lattice constants of  $\text{DySi}_2$  compared to  $\text{EuSi}_2$  [67] and, consequently, to smaller force constants in the latter [7]. The Dy-PDOS obtained along both orthogonal directions are identical, which stems from the orientation of the tetragonal  $\text{DySi}_2(001)$  unit cell on the  $\text{Si}(001)$  surface, namely, the z-axis being normal to the  $\text{Si}(001)$  [49]. It implies that in both orientations the wave vector of the x-rays remains in the  $xy$  plane, resulting in the identical Dy-PDOS.

The Dy-PDOS of the nanoislands [Fig. 1(a)] resembles that of sample A being, however, broader and shifted to lower energy. The main peak appears at 13 meV, and an increase of the number of low-energy phonon states is visible. The AFM image [Fig. 1(c)] shows isolated

rectangular nanoislands with an average width of 60 (10) nm and height of 22(2) nm [58].

The AFM image of sample *C* [Fig. 1(d)] reveals uniaxially aligned NWs along the steps ([1 $\bar{1}$ 0]) of the vicinal Si(001) surface with an average width of 6(1) nm, height of 0.7(2) nm, and lengths of several hundreds of nanometers [58], which are typical for these NWs [38,41,55]. Compared to the nanoislands, the Dy-PDOS of the NWs [Fig. 1(a)] exhibits a further shift to lower energy with a small peak at 7 meV, the main phonon states around 11 meV, and a high-energy tail between 15 and 18 meV. Furthermore, the Dy-PDOS along and across the NWs show a noticeable vibrational anisotropy between 9 and 12 meV with the number of states along the NWs exceeding those across the NWs.

We used the density functional theory, implemented in the VASP program [69], to investigate the lattice dynamics of DySi<sub>2</sub> in bulk, slab, and NW geometries. The calculations were performed within the generalized gradient approximation [70] and the projector augmented-wave potentials [71] with the 4*f* electrons of Dy placed in the core. The bulk tetragonal and hexagonal structures were studied using supercells with 48 atoms and lattice constants fixed to the experimental values [45–48]. The nanoislands were modeled using a Si-terminated tetragonal DySi<sub>2</sub>(001) slab. The NWs were investigated adopting the model of the TbSi<sub>2</sub> NWs [56] with lattice constants close to that of the Si(001) surface (3.84 Å). To calculate the Dy-induced (2 × 4) reconstructed Si surface between the NWs, which also contributes to the experimentally determined Dy-PDOS of sample *C*, we used the model reported for Yb atoms on the Si(001) [72]. Phonon dispersions and total and partial element-specific PDOS were calculated using the direct method [73] implemented in the PHONON program [74]. Figure 2 plots the total, element-, and direction-projected PDOS for the tetragonal bulk (a), slab (b), NWs (c), and the Dy-induced (2 × 4) reconstructed Si(001) surface (d). The corresponding crystal structures and the used *xyz* notation are also shown. In all configurations, the vibrations of the heavy Dy atoms contribute to the low-energy phonon states, whereas the vibrations of the lighter Si atoms extend to high energies. Further details are presented in Supplemental Material [58].

The experimental data were modeled with the *ab initio* calculated Dy-PDOS convoluted with the damped harmonic oscillator (DHO) function [75]. It introduces an energy-dependent broadening of the PDOS features, reflecting the fact that the phonons with higher energy (shorter wavelength) are strongly scattered (damped) by defects at surfaces and interfaces and within the nanostructures [8,76–78]. The DHO function is characterized by a quality factor *Q* which is inversely proportional to the damping strength. The following theoretical function was used:

$$g_{\text{theor}}(E) = N g_1(E, Q_1) + (1 - N) g_2(E, Q_2), \quad (1)$$

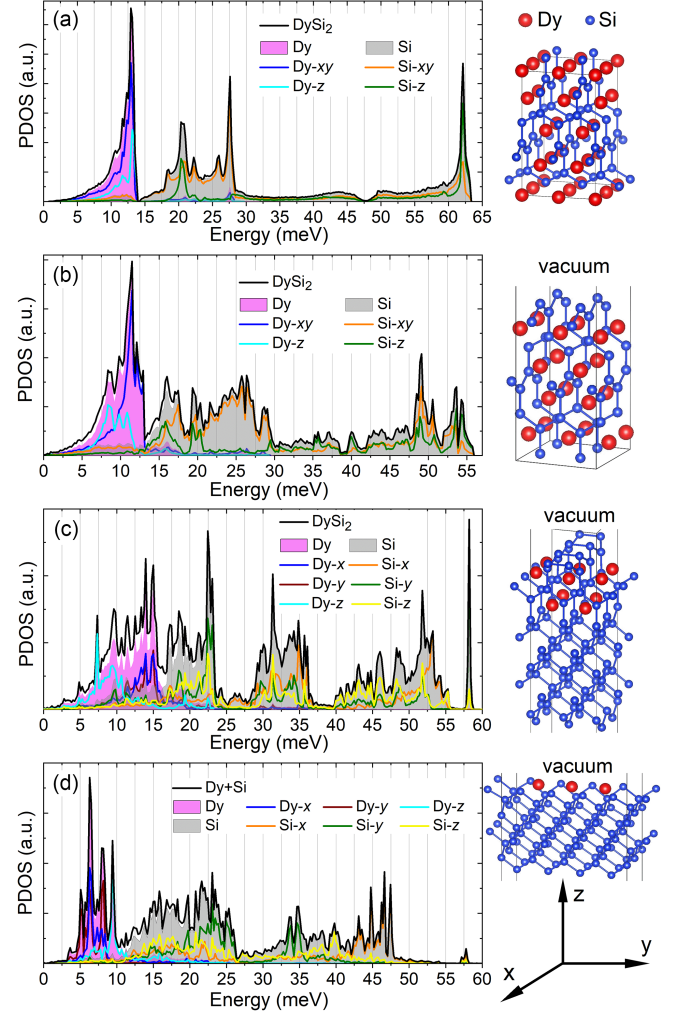


FIG. 2. The *ab initio* calculated total, Dy-, and Si-partial, *x*-, *y*-, and *z*-projected PDOS of DySi<sub>2</sub> in (a) tetragonal bulk, (b) tetragonal slab with a Si-terminated surface, (c) hexagonal NWs, and (d) Dy-induced (2 × 4) reconstructed Si(001) surface. The respective models of the corresponding crystal structures are shown next to each graph. The large red and small blue spheres stand for the Dy and Si atoms, respectively. The coordinate system defining the *x*, *y*, and *z* axes is also shown. In (a) and (b), these axes correspond to the main directions of the tetragonal DySi<sub>2</sub>. In (c), the *x* axis corresponds to the [0001] direction, whereas the *y* axis is along the [11 $\bar{2}$ 0] direction of the hexagonal DySi<sub>2</sub>. Additionally, in (c) and (d), *x* and *y* axes correspond to [1 $\bar{1}$ 0] and [110] directions, respectively, of the Si(001) surface.

with  $g_1(E, Q_1)$  and  $g_2(E, Q_2)$  being the corresponding *ab initio* calculated Dy-PDOS convoluted with the DHO function with the respective quality factors  $Q_1$  and  $Q_2$ ; *N* stands for the relative atomic fraction of the component described by  $g_1(E, Q_1)$ . The experimental data were modeled with  $g_{\text{theor}}(E)$  using the least-squares method with  $Q_1$ ,  $Q_2$ , and *N* being fit parameters.

The Dy-PDOS for both orientations of sample *A* were fully reproduced [Fig. 1(a)] using the *ab initio* calculated *xyz*-projected Dy-PDOS of tetragonal bulk DySi<sub>2</sub> [Fig. 2(a)]



TABLE I. The *ab initio* calculated Dy-PDOS  $g_1(E)$  and  $g_2(E)$  with the applied scaling factors (sc. fr.) to the energy axis along with the corresponding quality factors  $Q_1$  and  $Q_2$  of the DHO function and the relative fraction  $N$  of  $g_1(E)$  derived from the fit of Eq. (1) to the Dy-PDOS of the investigated samples for the given directions of the Si(001) surface.

Sample	$g_1(E)/\text{sc. fr.}$	$Q_1$	$g_2(E)/\text{sc. fr.}$	$Q_2$	$N$
A  Si[1 $\bar{1}$ 0]	$g_{\text{bulk-xyz}}^{\text{tetr}}/1.11$	13(1)	...	...	1.0
A  Si[110]	$g_{\text{bulk-xyz}}^{\text{tetr}}/1.11$	14(1)	...	...	1.0
B  Si[110]	$g_{\text{slab-xyz}}^{\text{tetr}}/1.17$	11(1)	...	...	1.0
C  Si[1 $\bar{1}$ 0]	$g_{\text{NWs-x}}^{\text{hex}}/0.79$	10(1)	$g_x^{(2 \times 4)}/1.10$	5(1)	0.82(1)
C  Si[110]	$g_{\text{NWs-y}}^{\text{hex}}/0.82$	11(1)	$g_y^{(2 \times 4)}/1.10$	10(1)	0.82(1)

convoluted with the DHO function (Table I). The contribution of  $z$ -polarized phonons originates from a small fraction of a polycrystalline DySi<sub>2</sub> evidenced by the sample characterization [58]. To match the position of the peak in the experimental PDOS, the energy axis of the theoretically obtained Dy-PDOS was multiplied by a scaling factor of 1.11, implying a shift toward higher energy. Although this shift could be a consequence from the compressive strain (4.95%) to which the DySi<sub>2</sub> tetragonal unit cell is subjected [49], an uncertainty in the *ab initio* calculated phonon frequencies arising from the approximations [58] adopted in the calculations cannot be excluded. The compressive strain field leads to formation of rectangular nanocrystals with a high fraction of grain boundaries [Fig. 1(b)] and to relatively low  $Q$  values, which are essentially the same for both directions (Table I).

Assuming a larger scaling factor and a smaller  $Q$  value as for sample A (Table I), the Dy-PDOS of sample B was reproduced [Fig. 1(a)] using the Dy-PDOS of the tetragonal DySi<sub>2</sub> slab [Fig. 2(b)]. Hence, the surface, near-surface, and a contribution of  $z$ -polarized phonons are the main origin of the excess of low- and high-energy states in the Dy-PDOS of sample B. Most likely, the contribution of phonons with  $z$  polarization arises from tilting of the nanoislands and lattice distortions which release the strain energy [50,51] and lead to the smaller  $Q$  value.

Attempts to reproduce the Dy-PDOS of sample C with the conventionally accepted NW orientation (length along the [1 $\bar{1}$ 20] and width along the [0001] directions) were not successful. Besides, regardless of the assumed orientation and applied scaling factors, the calculated Dy-PDOS of the NWs [Fig. 2(c)] alone could not account for the low-energy phonon states in the Dy-PDOS of sample C [Fig. 1(a)]. To fully comprehend the experimental data, one has to consider the fact that the NWs coexist with a Dy-induced (2  $\times$  4) and/or (2  $\times$  7) reconstructed Si(001) surface [52–54]. The formation of these reconstructions depends on the deposition conditions and impacts the width of the NWs [26]. Although we cannot directly identify the type of reconstruction present in sample C, the rather large width of

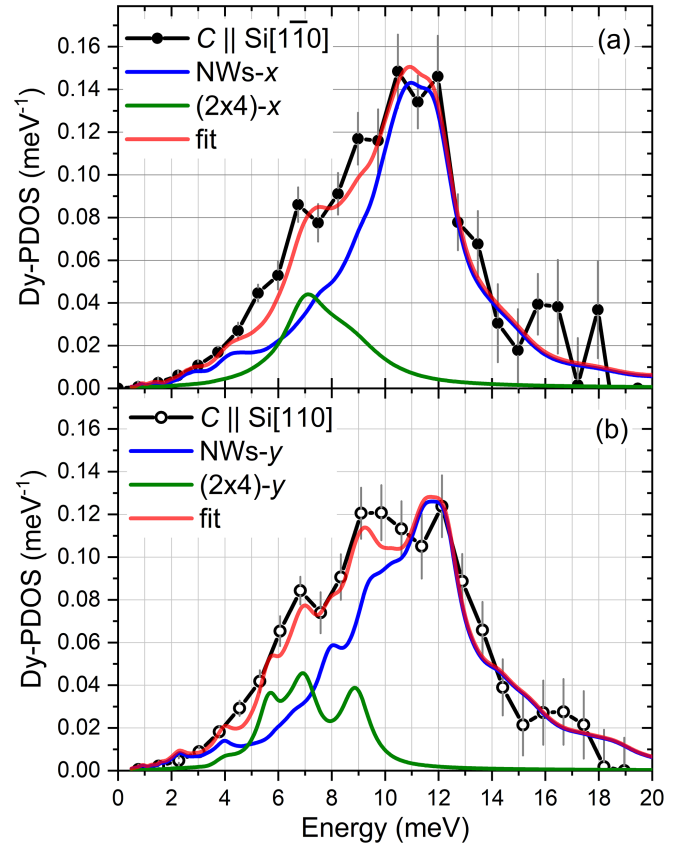


FIG. 3. The Dy-PDOS of the DySi<sub>2</sub> NWs obtained at 115 K with the wave vector of the x-rays being parallel (a) and perpendicular (b) to the NWs orientation [see Fig. 1(a)]. The fits of the theoretical function  $g_{\text{theor}}(E)$  [Eq. (1)] to the experimental data are also shown. The results from the fits are summarized in Table I (see the text for details).

the NWs, their high surface density (in part forming bundles of NWs), and the applied growth protocol suggest that the (2  $\times$  4) prevails over the (2  $\times$  7) reconstructed surface [58]. Taking into account that the NWs are orthogonal to the rows of Dy atoms forming the reconstruction [53], we modeled the experimental data with Eq. (1) assuming various orientations of the hexagonal unit cell of the NWs [58]. Opposite to the widely accepted model, the best fit of the Dy-PDOS along the NWs, depicted in Fig. 3(a), is obtained using the  $x$ -polarized Dy-PDOS of the NWs [Fig. 2(c)], which corresponds to the [0001] direction, and the  $x$ -polarized Dy-PDOS of the (2  $\times$  4) reconstruction [Fig. 2(d)]. The Dy-PDOS across the NWs [Fig. 3(b)] is best reproduced by the  $y$ -polarized Dy-PDOS of the NWs [Fig. 2(c)], corresponding to the [1 $\bar{1}$ 20] direction, and the  $y$ -polarized Dy-PDOS of the (2  $\times$  4) reconstruction [Fig. 2(d)]. The applied scaling factors and the derived values of  $Q$  and  $N$  are presented in Table I. The shift of the theoretical Dy-PDOS of the NWs [(2  $\times$  4) reconstruction] to lower (higher) energy indicates that these scaling factors do not correlate with the epitaxial strain. Most likely, they

arise from various approximations adopted in calculations of the electronic properties and the structural models without crystal defects [58]. The values of  $Q$  are close to that of sample *B*, except for the  $(2 \times 4)$ - $x$ , which is reduced by a factor of 2, likely due to the very sharp peak in the theoretical Dy-PDOS [Fig. 2(d)]. Furthermore, in addition to the epitaxial strain field, Si vacancies that exist in real RESi<sub>2</sub> structures [48,79] might contribute to the relatively low  $Q$  values of all samples, which are comparable to those obtained in similar systems [76,77]. In agreement with the high surface density of the NWs [58], the obtained from the fit atomic fraction  $N$  (Table I) shows that the amount of Dy atoms forming the NWs dominate those of the  $(2 \times 4)$  reconstruction. Notably,  $N$  assumes the same value for both orientations, which highlights the consistency of the model.

The remarkable agreement between experiment and theory, presented in Fig. 3, demonstrates that, opposite to the previously proposed anisotropic mismatch model [24], the DySi<sub>2</sub> NWs are formed with their length along the [0001] and width along the [11 $\bar{2}$ 0] directions of the hexagonal unit cell. This conclusion is supported by the refined structure model of TbSi<sub>2</sub> NWs [56,57]. The Dy-PDOS of sample *C* shows an almost identical high-energy cutoff for both orientations [Fig. 1(a)], which is clear evidence for very similar interatomic distances along the investigated crystallographic directions. To shed light on the effect of the lattice parameters on the PDOS of the NWs, we performed *ab initio* calculations assuming the lattice constants of bulk hexagonal DySi<sub>2</sub> [48]. The results [58] demonstrate that, in addition to the vibrational anisotropy, a significant low-energy shift of the Dy-PDOS along the direction with the higher lattice constant is to be expected, which is not confirmed experimentally. Hence, for both orthogonal directions, the NWs exhibit very similar in-plane lattice parameters, which are close to that of the Si(001) surface. Most likely, the height of the NWs of only two layers of rare earth atoms is not sufficient for strain relaxation and establishing the lattice parameters of bulk hexagonal DySi<sub>2</sub>.

The modified Dy-PDOS of DySi<sub>2</sub> upon the transition from the bulk to nanoislands and NWs leads to alterations of their thermodynamic and elastic properties presented in Table II. The lattice specific heat capacity and vibrational entropy of the nanoislands increase by 1% and 7%, respectively, whereas in the NWs the corresponding deviations reach 5% and 27% compared to the bulk values. In average, the mean force constant decreases by 8% in the nanoislands and 33% in the NWs compared to sample *A*, whereas the mean square displacement of the Dy atoms increases by 19% and 66%, respectively. However, one has to notice that the Dy atoms forming the  $(2 \times 4)$  reconstruction (Table I) also contribute to these deviations in sample *C*. The small vibrational anisotropy in the

TABLE II. Lattice specific heat capacity at constant volume  $C_V$  ( $k_B$  per atom), vibrational entropy  $S_V$  ( $k_B$  per atom), mean force constant  $F$  (Nm<sup>-1</sup>), and mean square displacement  $\langle x^2 \rangle$  (Å<sup>2</sup>) of the Dy atoms obtained from the Dy-PDOS of the investigated samples at 115 K for the given directions of the Si(001) surface.

Sample	$C_V$	$S_V$	$F$	$\langle x^2 \rangle$
A  Si[1 $\bar{1}$ 0]	2.59(2)	2.49(2)	109(2)	0.0024(1)
A  Si[110]	2.60(2)	2.49(2)	108(2)	0.0023(1)
B  Si[110]	2.63(2)	2.66(2)	100(3)	0.0028(2)
C  Si[1 $\bar{1}$ 0] (along NWs)	2.73(3)	3.16(3)	72(3)	0.0038(3)
C  Si[110] (across NWs)	2.72(3)	3.16(3)	74(3)	0.0040(3)

Dy-PDOS of the NWs leads to marginal differences of these properties along the orthogonal directions.

In summary, using *in situ* nuclear inelastic scattering on <sup>161</sup>Dy we determined the lattice dynamics, thermodynamic, and elastic properties of epitaxial DySi<sub>2</sub> upon the transition from the bulk to self-organized nanoislands and NWs on the vicinal Si(001) surface. Compared to the bulk, the nanoislands exhibit softening of the crystal lattice, which is further enhanced in the NWs and significantly affects their thermodynamic and elastic properties. Our *ab initio* calculations reveal that this effect originates from the vibrations of atoms located at the surfaces of the nanoislands and the NWs and between them, forming a  $(2 \times 4)$  reconstruction. The comparison between experiment and theory demonstrates that, opposite to the widely accepted anisotropic lattice mismatch model, the DySi<sub>2</sub> NWs are formed with their length along the [0001] and their width along the [11 $\bar{2}$ 0] directions of the strained hexagonal unit cell. Very likely, this applies to the other RESi<sub>2</sub> NWs.

These results shed new light on the structural characteristics and vibrational dynamics of the self-organized RESi<sub>2</sub> nanoislands and NWs that may facilitate precise predictive modeling of their fundamental properties and advance their applications. Furthermore, our results reveal that, unlike the bulklike vibrational dynamics [76,77] of endotaxial [80] nanostructures, the vibrational properties of the RESi<sub>2</sub> nanostructures are governed by their surfaces, which is a prerequisite for enhanced interactions of phonons with electrons, magnons, and other phonons [11,12]. Hence, by a careful tuning of the growth regime of the nanostructures, one is able to enhance or suppress these interactions. Potentially, this could advance fields like thermoelectric energy conversion, thermal management, spintronics, and quantum computing.

*Acknowledgments*—S. S. acknowledges the financial support from the Helmholtz Association (No. VH-NG-625) and the Federal Ministry of Education and Research BMBF (No. 05K22VK2). P. P. acknowledges the Polish Ministry of Science and Higher Education—Decision No. 2021/WK/11 for financing the access to the ESRF. We acknowledge ESRF-The European Synchrotron for

provision of synchrotron radiation facilities at the Nuclear Resonance beamline ID18 (Exp. MA-2174) and the National Isotope Development Center at Oak Ridge National Lab, which is sponsored by the U.S. DOE Basic Energy Sciences, for providing the  $^{161}\text{Dy}$ . We thank J.-Ph. Celse for the support at the ESRF and B. Krause and A. Weißhardt for the support at the KIT.

**Data availability**—The data that support the findings of this article are not publicly available. The data are available from the authors upon reasonable request.

- [1] G. P. Srivastava, *The Physics of Phonons*, 1st ed. (CRC Press, Boca Raton, 1990).
- [2] B. Fultz, Vibrational thermodynamics of materials, *Prog. Mater. Sci.* **55**, 247 (2010).
- [3] M. A. Strocio and M. Dutta, *Phonons in Nanostructures*, 1st ed. (Cambridge University Press, Cambridge, England, 2001).
- [4] S. Stankov, R. Röhlberger, T. Ślęzak, M. Sladeczek, B. Sepiol, G. Vogl, A. I. Chumakov, R. Rüffer, N. Spiridis, J. Łażewski, K. Parliński, and J. Korecki, Phonons in iron: From the bulk to an epitaxial monolayer, *Phys. Rev. Lett.* **99**, 185501 (2007).
- [5] T. Ślęzak, J. Łażewski, S. Stankov, K. Parlinski, R. Reitering, M. Rennhofer, R. Rüffer, B. Sepiol, M. Ślęzak, N. Spiridis, M. Zajac, A. I. Chumakov, and J. Korecki, Phonons at the Fe(110) surface, *Phys. Rev. Lett.* **99**, 066103 (2007).
- [6] B. Roldan Cuenya, W. Keune, R. Peters, E. Schuster, B. Sahoo, U. von Hörsten, W. Sturhahn, J. Zhao, T. S. Toellner, E. E. Alp, and S. D. Bader, High-energy phonon confinement in nanoscale metallic multilayers, *Phys. Rev. B* **77**, 165410 (2008).
- [7] A. Seiler, P. Piekarczyk, S. Ibrahimkuty, D. G. Merkel, O. Waller, R. Pradip, A. I. Chumakov, R. Rüffer, T. Baumbach, K. Parlinski, M. Fiederle, and S. Stankov, Anomalous lattice dynamics of  $\text{EuSi}_2$  nanoislands: Role of interfaces unveiled, *Phys. Rev. Lett.* **117**, 276101 (2016).
- [8] J. Kalt, M. Sternik, I. Sergueev, J. Herfort, B. Jenichen, H.-C. Wille, O. Sikora, P. Piekarczyk, K. Parlinski, T. Baumbach, and S. Stankov, Lattice dynamics of epitaxial strain-free interfaces, *Phys. Rev. B* **98**, 121409(R) (2018).
- [9] R. Pradip, P. Piekarczyk, D. G. Merkel, J. Kalt, O. Waller, A. I. Chumakov, R. Rüffer, A. M. Oleś, K. Parlinski, T. Baumbach, and S. Stankov, Phonon confinement and spin-phonon coupling in tensile-strained ultrathin  $\text{EuO}$  films, *Nanoscale* **11**, 10968 (2019).
- [10] S. Stankov, D. G. Merkel, J. Kalt, J. Göttlicher, J. Łażewski, M. Sternik, P. T. Jochym, P. Piekarczyk, T. Baumbach, A. I. Chumakov, and R. Rüffer, Phonon confinement and interface lattice dynamics of ultrathin high- $k$  rare earth sesquioxide films: The case of  $\text{Eu}_2\text{O}_3$  on  $\text{YSZ}(001)$ , *Nanoscale Adv.* **4**, 19 (2022).
- [11] D. Bozyigit, N. Yazdani, M. Yarema, O. Yarema, W. M. M. Lin, S. Volk, K. Vuttivorakulchai, M. Luisier, F. Juranyi, and V. Wood, Soft surfaces of nanomaterials enable strong phonon interactions, *Nature (London)* **531**, 618 (2016).
- [12] C. Berk, M. Jaris, W. Yang, S. Dhuey, S. Cabrini, and H. Schmidt, Strongly coupled magnon–phonon dynamics in a single nanomagnet, *Nat. Commun.* **10**, 2652 (2019).
- [13] J. Chen, X. Xu, J. Zhou, and B. Li, Interfacial thermal resistance: Past, present, and future, *Rev. Mod. Phys.* **94**, 025002 (2022).
- [14] J. P. Pekola and B. Karimi, Colloquium: Quantum heat transport in condensed matter systems, *Rev. Mod. Phys.* **93**, 041001 (2021).
- [15] S. Bandyopadhyay, *Introduction to Spintronics*, 2nd ed. (CRC Press, Boca Raton, 2015).
- [16] N. Li, J. Ren, L. Wang, G. Zhang, P. Hänggi, and B. Li, Colloquium: Phononics: Manipulating heat flow with electronic analogs and beyond, *Rev. Mod. Phys.* **84**, 1045 (2012).
- [17] A. A. Balandin and D. L. Nika, Phononics in low-dimensional materials, *Mater. Today* **15**, 266 (2012).
- [18] S. Volz *et al.*, Nanophononics: State of the art and perspectives, *Eur. Phys. J. B* **89**, 15 (2016).
- [19] M. Jansen, W. A. Tisdale, and V. Wood, Nanocrystal phononics, *Nat. Mater.* **22**, 161 (2023).
- [20] *CMOS Nanoelectronics Innovative Devices, Architectures, and Applications*, edited by N. Collaert, 1st ed. (Jenny Stanford Publishing, Singapore, 2012).
- [21] S. Bandyopadhyay, *Physics of Nanostructured Solid State Devices*, 1st ed. (Springer Science and Business Media, New York, 2012).
- [22] J. Yao, H. Yan, S. Das, J. F. Klemic, J. C. Ellenbogen, and C. M. Lieber, Nanowire nanocomputer as a finite-state machine, *Proc. Natl. Acad. Sci. U.S.A.* **111**, 2431 (2014).
- [23] C. Preinesberger, S. Vandr , T. Kalka, and M. D hne-Prietsch, Formation of dysprosium silicide wires on Si (001), *J. Phys. D* **31**, L43 (1998).
- [24] Y. Chen, D. A. A. Ohlberg, G. Medeiros-Ribeiro, Y. A. Chang, and R. S. Williams, Self-assembled growth of epitaxial erbium disilicide nanowires on silicon (001), *Appl. Phys. Lett.* **76**, 4004 (2000).
- [25] Y. Chen, D. A. A. Ohlberg, and R. S. Williams, Nanowires of four epitaxial hexagonal silicides grown on Si(001), *J. Appl. Phys.* **91**, 3213 (2002).
- [26] Y. Cui, J. Chung, and J. Nogami, Controlling the width of self-assembled dysprosium silicide nanowires on the Si (001) surface, *J. Phys. Condens. Matter* **24**, 045003 (2012).
- [27] M. D hne and M. Wanke, Metallic rare-earth silicide nanowires on silicon surfaces, *J. Phys. Condens. Matter* **25**, 014012 (2013).
- [28] D. E. Chang, A. S. S rensen, P. R. Hemmer, and M. D. Lukin, Quantum optics with surface plasmons, *Phys. Rev. Lett.* **97**, 053002 (2006).
- [29] G. S. Snider and R. S. Williams, Nano/CMOS architectures using a field-programmable nanowire interconnect, *Nanotechnology* **18**, 035204 (2007).
- [30] I. Miccoli, F. Edler, H. Pfn r, S. Appelfeller, M. D hne, K. Holtgrewe, S. Sanna, W. G. Schmidt, and C. Tegenkamp, Atomic size effects studied by transport in single silicide nanowires, *Phys. Rev. B* **93**, 125412 (2016).
- [31] H. Pfn r *et al.*, Atomic wires on substrates: Physics between one and two dimensions, *Surf. Sci. Rep.* **79**, 100629 (2024).
- [32] H. W. Yeom, Y. K. Kim, E. Y. Lee, K.-D. Ryang, and P. G. Kang, Robust one-dimensional metallic band structure of silicide nanowires, *Phys. Rev. Lett.* **95**, 205504 (2005).



- [33] M. Wanke, K. Löser, G. Pruskil, D. V. Vyalikh, S. L. Molodtsov, S. Danzenbächer, C. Laubschat, and M. Dähne, Electronic properties of self-assembled rare-earth silicide nanowires on Si(001), *Phys. Rev. B* **83**, 205417 (2011).
- [34] S. Appelfeller, M. Franz, H.-F. Jirschik, J. Große, and M. Dähne, The electronics structure of Tb silicide nanowires on Si(001), *New J. Phys.* **18**, 113005 (2016).
- [35] K. Holtgrewe, S. Appelfeller, M. Franz, M. Dähne, and S. Sanna, Structure and one-dimensional metallicity of rare-earth silicide nanowires on Si(001), *Phys. Rev. B* **99**, 214104 (2019).
- [36] C. Zeng, P. R. C. Kent, T.-H. Kim, A.-P. Li, and H. H. Weitering, Charge-order fluctuations in one-dimensional silicides, *Nat. Mater.* **7**, 539 (2008).
- [37] S. Sanna, J. Plaickner, K. Holtgrewe, V. M. Wettig, E. Speiser, S. Chandola, and N. Esser, Spectroscopic analysis of rare-earth silicide structures on the Si(111) surface, *Materials* **14**, 4104 (2021).
- [38] C. Preinesberger, S. K. Becker, S. Vandr , T. Kalka, and M. Dähne, Structure of DySi<sub>2</sub> nanowires on Si(001), *J. Appl. Phys.* **91**, 1695 (2002).
- [39] Z. He, M. Stevens, D. J. Smith, and P. A. Bennett, Dysprosium silicide nanowires on Si(110), *Appl. Phys. Lett.* **83**, 5292 (2003).
- [40] B. Z. Liu and J. Nogami, Growth of parallel rare-earth silicide nanowire arrays on vicinal Si(001), *Nanotechnology* **14**, 873 (2003).
- [41] C. Preinesberger, G. Pruskil, S. K. Becker, M. Dähne, D. V. Vyalikh, S. L. Molodtsov, C. Laubschat, and F. Schiller, Structure and electronic properties of dysprosium-silicide nanowires on vicinal Si(001), *Appl. Phys. Lett.* **87**, 083107 (2005).
- [42] M. Wanke, K. Löser, G. Pruskil, and M. Dähne, Structural and electronic properties of rare earth silicide nanowires on Si(557), *Phys. Rev. B* **79**, 155428 (2009).
- [43] M. Wanke, M. Franz, M. Vetterlein, G. Pruskil, C. Prohl, B. Höpfner, P. Stojanov, E. Huwald, J. D. Riley, and M. Dähne, Electronic properties of dysprosium silicide nanowires on Si(557), *J. Appl. Phys.* **108**, 064304 (2010).
- [44] A. Seiler, S. Ibrahimkuty, P. Wochner, R. Pradip, O. Waller, B. Krause, A. Plech, T. Baumbach, M. Fiederle, and S. Stankov, Thermal stability studies of DySi<sub>2</sub> nanowires and nanoislands by in Situ GISAXS, *J. Phys. Chem. C* **120**, 7365 (2016).
- [45] J. Perri, E. Banks, and B. Post, Polymorphism of rare earth disilicides, *J. Phys. Chem.* **63**, 2073 (1959).
- [46] V. Eremenko, K. Meleshevich, Y. Buyanov, and P. Martsenyuk, Structure, composition and phase equilibria in dysprosium silicon alloys, *Ukr. Khim. Zh. (Russ. Ed.)* **60**, 544 (1994).
- [47] K. Xu, L. Chen, K. Chang, P. Wan, M. Li, Z. Deng, F. Huang, and Q. Huang, Thermodynamic description of the Dy–Si–C system in silicon carbide ceramics, *CALPHAD: Comput. Coupling Phase Diagrams Thermochem.* **68**, 101738 (2020).
- [48] V. Koleshko, V. Belitsky, and A. Khodin, Thin films of rare earth metal silicides, *Thin Solid Films* **141**, 277 (1986).
- [49] A. Travlos, N. Salamouras, and N. Boukos, Epitaxial dysprosium silicide films on silicon: Growth, structure and electrical properties, *Thin Solid Films* **397**, 138 (2001).
- [50] G. Ye, M. A. Crimp, and J. Nogami, Crystallographic study of self-assembled dysprosium silicide nanostructures on Si(001), *Phys. Rev. B* **74**, 033104 (2006).
- [51] G. Ye, J. Nogami, and M. A. Crimp, Dysprosium disilicide nanostructures on silicon(001) studied by scanning tunneling microscopy and transmission electron microscopy, *Thin Solid Films* **497**, 48 (2006).
- [52] B. Liu and J. Nogami, An STM study of the Si(001) (2 × 4)-Dy surface, *Surf. Sci.* **488**, 399 (2001).
- [53] B. Liu and J. Nogami, An STM study of the Si(001) (2 × 7)-Gd, Dy surface, *Surf. Sci.* **540**, 136 (2003).
- [54] B. Z. Liu and J. Nogami, A scanning tunneling microscopy study of dysprosium silicide nanowire growth on Si(001), *J. Appl. Phys.* **93**, 593 (2003).
- [55] J. Nogami, B. Z. Liu, M. V. Katkov, C. Ohbuchi, and N. O. Birge, Self-assembled rare-earth silicide nanowires on Si(001), *Phys. Rev. B* **63**, 233305 (2001).
- [56] S. Appelfeller, J. Heggemann, T. Niermann, M. Lehmann, and M. Dähne, Refined structure model of rare earth silicide nanowires on Si(001), *Appl. Phys. Lett.* **114**, 093104 (2019).
- [57] J. Heggemann, S. Appelfeller, T. Niermann, M. Lehmann, and M. Dähne, Internal atomic structure of terbium silicide nanowires on Si(001) capped by silicon, *Surf. Sci.* **696**, 121563 (2020).
- [58] See Supplemental Material at <http://link.aps.org/supplemental/10.1103/4r3t-tr77>, which includes Ref. [59], for further details about sample preparation and characterization, *ab initio* lattice dynamics calculations, and additional fit results of the PDOS of the NWs.
- [59] I. Semitelou, A two-phase magnetic structure of DySi<sub>2</sub>, *J. Magn. Magn. Mater.* **267**, 42 (2003).
- [60] M. Seto, Y. Yoda, S. Kikuta, X. W. Zhang, and M. Ando, Observation of nuclear resonant scattering accompanied by phonon excitation using synchrotron radiation, *Phys. Rev. Lett.* **74**, 3828 (1995).
- [61] W. Sturhahn, T. S. Toellner, E. E. Alp, X. Zhang, M. Ando, Y. Yoda, S. Kikuta, M. Seto, C. W. Kimball, and B. Dabrowski, Phonon density of states measured by inelastic nuclear resonant scattering, *Phys. Rev. Lett.* **74**, 3832 (1995).
- [62] S. Stankov, R. Rüffer, M. Sladeczek, M. Rennhofer, B. Sepiol, G. Vogl, N. Spiridis, T. Slezak, and J. Korecki, An ultrahigh vacuum system for in situ studies of thin films and nanostructures by nuclear resonance scattering of synchrotron radiation, *Rev. Sci. Instrum.* **79**, 045108 (2008).
- [63] R. Rüffer and A. I. Chumakov, Nuclear resonance beamline at ESRF, *Hyperfine Interact.* **97**, 589 (1996).
- [64] A. I. Chumakov, R. Rüffer, O. Leupold, A. Barla, H. Thiess, J. M. Gil, H. V. Alberto, R. C. Vil o, N. Ayres de Campos, V. G. Kohn, M. Gerken, and M. Lucht, Nuclear inelastic scattering with <sup>161</sup>Dy, *Phys. Rev. B* **63**, 172301 (2001).
- [65] A. I. Chumakov and W. Sturhahn, Experimental aspects of inelastic nuclear resonance scattering, *Hyperfine Interact.* **123**, 781 (1999).

- [66] A. I. Chumakov and V. G. Kohn, DOS: Evaluation of phonon density of states from nuclear resonant inelastic absorption, *Hyperfine Interact.* **125**, 205 (2000).
- [67] J. A. Perri, I. Binder, and B. Post, Rare earth “disilicides,” *J. Phys. Chem.* **63**, 616 (1959).
- [68] J.-C. G. Bunzli and V. K. Pecharsky, *Handbook on the Physics and Chemistry of Rare Earths: Including Actinides* (Elsevier, New York, 2016).
- [69] G. Kresse and J. Furthmüller, Efficiency of ab-initio total energy calculations for metals and semiconductors using a plane-wave basis set, *Comput. Mater. Sci.* **6**, 15 (1996).
- [70] J. P. Perdew, K. Burke, and M. Ernzerhof, Generalized gradient approximation made simple, *Phys. Rev. Lett.* **77**, 3865 (1996).
- [71] P. E. Blöchl, Projector augmented-wave method, *Phys. Rev. B* **50**, 17953 (1994).
- [72] M. Kuzmin, M. P. J. Punkkinen, P. Laukkanen, R. E. Perälä, M. Ahola-Tuomi, T. Balasubramanian, and I. J. Värynen, Yb-induced ( $2 \times 3$ ) and ( $2 \times 4$ ) reconstructions on Si(100) studied by first-principles calculations and high-resolution core-level photoelectron spectroscopy, *Phys. Rev. B* **78**, 045318 (2008).
- [73] K. Parlinski, Z. Q. Li, and Y. Kawazoe, First-principles determination of the soft mode in cubic  $\text{ZrO}_2$ , *Phys. Rev. Lett.* **78**, 4063 (1997).
- [74] K. Parlinski, Software PHONON, Cracow, 2021.
- [75] B. Fåk and B. Dorner, Institute Laue Langevin Technical, Report No. 92FA008S, 1992 (unpublished).
- [76] J. Kalt, M. Sternik, B. Krause, I. Sergueev, M. Mikolasek, D. Merkel, D. Bessas, O. Sikora, T. Vitova, J. Göttlicher, R. Steininger, P. T. Jochym, A. Ptok, O. Leupold, H.-C. Wille, A. I. Chumakov, P. Piekarz, K. Parlinski, T. Baumbach, and S. Stankov, Lattice dynamics of endotaxial silicide nanowires, *Phys. Rev. B* **102**, 195414 (2020).
- [77] J. Kalt, M. Sternik, B. Krause, I. Sergueev, M. Mikolasek, D. Bessas, O. Sikora, T. Vitova, J. Göttlicher, R. Steininger, P. T. Jochym, A. Ptok, O. Leupold, H.-C. Wille, A. I. Chumakov, P. Piekarz, K. Parlinski, T. Baumbach, and S. Stankov, Lattice dynamics and polarization-dependent phonon damping in  $\alpha$ -phase  $\text{FeSi}_2$  nanostructures, *Phys. Rev. B* **101**, 165406 (2020).
- [78] J. Kalt, M. Sternik, I. Sergeev, M. Mikolasek, D. Bessas, J. Göttlicher, B. Krause, T. Vitova, R. Steininger, O. Sikora, P. T. Jochym, O. Leupold, H.-C. Wille, A. I. Chumakov, P. Piekarz, K. Parlinski, T. Baumbach, and S. Stankov, Lattice dynamics of  $\beta$  –  $\text{FeSi}_2$  nanorods, *Phys. Rev. B* **106**, 205411 (2022).
- [79] L. Magaud, A. Pasturel, G. Kresse, and J. Hafner, Role of silicon vacancies in yttrium-disilicide compounds from ab initio calculations, *Phys. Rev. B* **55**, 13479 (1997).
- [80] Z. He, D. J. Smith, and P. A. Bennett, Endotaxial silicide nanowires, *Phys. Rev. Lett.* **93**, 256102 (2004).